

## Article

# Large Eddy Simulations on Film Cooling Flow Behaviors with Upstream Turbulent Boundary Layer Generated by Circular Cylinder

Young Seok Kang <sup>1,\*</sup>, Dong-Ho Rhee <sup>1</sup>, Yu Jin Song <sup>2</sup> and Jae Su Kwak <sup>2</sup> <sup>1</sup> Aeropropulsion Research Division, Korea Aerospace Research Institute, Daejeon 34133, Korea; rhee@kari.re.kr<sup>2</sup> School of Aerospace and Mechanical Engineering, Korea Aerospace University, Goyang 10540, Korea; yujin0963@kau.kr (Y.J.S.); jskwak@kau.ac.kr (J.S.K.)

\* Correspondence: electra@kari.re.kr

**Abstract:** Large eddy simulations on film cooling hole array on a flat plate was carried out to investigate upstream turbulence effect. Circular cylinders were configured to create a turbulent boundary layer and its diameter has been adjusted to generate 13% upstream turbulence intensity in the main flow. Due to the small pitch to diameter configuration of the cylinder, two-dimensional LES analysis was carried out in advance and the results showed that LES was an essential method to resolve flow field around and downstream circular cylinder, which was not available in RANS simulations. The three-dimensional LES results showed reasonable agreement in turbulence intensity and normalized velocity distributions along the vertical with measured data. According to the blowing ratio, the cooling flow coverage on the surface along the stream-wise direction was varied and well agreed with measured data. Additionally, upstream boundary flows were partially ingested inside the cooling hole and discharged again near along the centerline of the cooling hole. This accounted for film cooling effectiveness distribution inside the cooling hole surface and along the centerline. The current study revealed that the LES for predicting turbulent boundary layer behaviors due to upstream turbulence generation source was an effective and feasible method. Moreover, the LES effectively resolved flow fields such as film cooling flow behaviors and corresponding film cooling effectiveness distributions.

**Keywords:** film cooling hole; large eddy simulation; gas turbine; cooling turbine



**Citation:** Kang, Y.S.; Rhee, D.-H.; Song, Y.J.; Kwak, J.S. Large Eddy Simulations on Film Cooling Flow Behaviors with Upstream Turbulent Boundary Layer Generated by Circular Cylinder. *Energies* **2021**, *14*, 7227. <https://doi.org/10.3390/en14217227>

Academic Editor: Flavio Caresana

Received: 20 July 2021

Accepted: 21 October 2021

Published: 2 November 2021

**Publisher's Note:** MDPI stays neutral with regard to jurisdictional claims in published maps and institutional affiliations.



**Copyright:** © 2021 by the authors. Licensee MDPI, Basel, Switzerland. This article is an open access article distributed under the terms and conditions of the Creative Commons Attribution (CC BY) license (<https://creativecommons.org/licenses/by/4.0/>).

## 1. Introduction

To improve gas turbine engine performances such as specific power and efficiency, the turbine inlet temperature of the gas turbine should be increased. General Ni alloy, widely used for the hot section in the modern gas turbine, can withstand up to 950 °C without cooling. However, since the turbine inlet temperature exceeds the temperature that the material can withstand, appropriate cooling methods should be applied. Film cooling is one of the external cooling technologies generally applied to hot sections in the gas turbine. Low-temperature cooling flow is injected and pasted over the turbine blade surface to form a thin film layer, which protects the blade surface from high-temperature working fluids.

To evaluate film cooling performance by numerical method, the Reynolds Averaged Navier-Stokes (RANS) analysis method has been widely used, because of its efficiency in computational costs. In many cases, however, RANS analysis results showed less accuracy compared to Large Eddy Simulation (LES) results [1–3]. In the meanwhile, LES directly resolves grid-scale eddies and resultant flow perturbation in the control volume, which are not available in the RANS method. Mostly, LES shows higher accuracy than RANS in the flow field where resolved eddies have dominant effects on the flow field, such as cooling flow behaviors injected from the film cooling hole. For this reason, LES has been highlighted because of its usefulness for analyzing flow fields around film cooling holes.

Two previous researches showed that there were discrepancies between LES results and experimental data for predicting film cooling flow injected from a well-known 7-7-7 fan shaped film cooling hole [2,3]. Both researches showed that on the lateral side of the 7-7-7 cooling hole, there appeared a high film cooling effectiveness region, which was not shown in the experimental data. It was thought that the cooling flow injected to the lateral side of the film cooling hole did not lift off and protected the wall while maintaining a stable vortex structure. Meanwhile, Tracy and Lynch used a trip strip to generate turbulent boundary layer upstream of the 7-7-7 shaped film cooling hole with axial and compound angle orientations. They obtained reasonable turbulent velocity profile in front of the cooling hole and film cooling effectiveness distributions on a flat plate close to experimental data [4].

Judging from the results of previous studies mentioned above, as flow fields of the combustor and turbine in gas turbines usually experience very high turbulent flows, methods are required to introduce turbulence information when using the LES method to predict problem-dependent eddies in the simulation and its effects on combustor and turbine performances. Therefore, various techniques have been devised to provide turbulence information to the inlet boundary conditions when analyzing these components with the LES method. From previous researches, methods to give turbulence information at the inlet boundary of LES analysis could be categorized as follows:

- Flow recycling
- Transient boundary table
- Synthetic turbulence generation
- Obstacle geometry to generate turbulence

One of the methods is the inlet boundary recycling method which has been widely used to introduce turbulence information at the inlet boundary. It is a classic method consisting of recycling outflow to inflow in a flat plate flow until the boundary layer develops to fully turbulent; the number of flow recirculation could be evaluated by Reynolds number based on the flat plate length. However, this method still requires a lot of computational costs. For this reason, to reduce the required flow recirculation cycle and corresponding computational costs, advanced methods to develop early transition of the boundary layer have been also reported. Jee et al. [5] introduced cost effective boundary layer transition method by introducing primary instability and subharmonic perturbations. The transient boundary table method was also found to be an effective method to give turbulence information in LES analysis [6]. Flow field from existing CFD results (LES/DNS or other scale resolving simulation), which contain turbulence information, are specified as an inlet boundary condition in another LES calculation. Synthetic turbulence generation methods, which introduce turbulence information at the chosen inlet boundary surface, were also evaluated to be effective for early transition of the boundary layer [7,8]. In general, random function, distribution function, and Reynolds stress information are required to generate turbulence information.

Alternatively, implementing obstacle geometry in the computational domain at the upstream of the flow domain of interest is an effective method to introduce turbulence information in the boundary layer. Trip strip configuration by varying its location and size was found to be effective for implementing the required boundary layer characteristic in front of the cooling hole [4,9]. These previous researches used rectangular trip strips of which sizes were order of the cooling hole.

Meanwhile, several experimental researches used turbulator whose dimension is larger than the geometry of interests to generate high turbulence intensity in the experimental environment [10]. For example, circular cylinders have been widely used in experiments in front of the test section for generating turbulence. According to the Reynolds number based on the cylinder diameter and main flow velocity and its correlation with Strouhal number, von Karman vortex street is generating around the circular cylinder and dissipating behind the circular cylinder. It is suggested that, to simulate a physically valid flow field around the circular cylinder, scale resolving simulations such as DES and LES are

recommended [11]. A row of the circular cylinders was configured to experimentally assess film cooling performance by strong turbulent boundary layer [12]. However, there has been no effort to numerically assess the film cooling performance with such a configuration. For this reason, there is still no clear understanding of the strong main flow turbulent boundary layer effects on the flow field near the cooling hole and cooling performance.

In this study, a row of the circular cylinder was included in the computational domain as in the experiment to generate strong turbulence over 10% turbulence intensity in the main flow. The von Karman vortex street was continuously generated and dissipated downstream of the cylinder which is the main source of velocity perturbations and corresponding turbulent boundary layer in the main flow. The main objectives of this study were to numerically assess the strong upstream turbulent boundary layer effect on the film cooling flow behavior and cooling performance over the flat plate and to assess the feasibility of the LES method for the capability to resolve interaction between the strong turbulent boundary layer and film cooling flow.

## 2. Description of Film Cooling Hole

The geometry of a fan-shaped film cooling hole for this study was designed by Seo et al. [13]. The fan-shaped film cooling hole has been optimized with the RANS-based numerical simulation method based on a well-known 7-7-7 fan-shaped film cooling hole presented by Shroeder and Thole [14]. The design points for the optimization were derived by the Box–Behnken design, which is a design of experiments (DOE) for response surface methodology (RSM). RANS simulations for each experimental point were carried out when both the blowing ratio and density ratio are 2.0. Three shape parameters of a fan-shaped hole were selected as design variables: the forward expansion angle ( $\beta_{fwd}$ ), the lateral expansion angle ( $\beta_{lat}$ ), and metering length ratio ( $L_m/D$ ). The hole length to diameter ratio ( $L/D$ ) was fixed at 6. The area-averaged film cooling effectiveness was selected as an objective function. In the optimized design, the forward expansion angle, and the lateral expansion angle of the optimized hole and metering length ratio were 13.3 degrees, 13 degrees, and 2, respectively. The shape of the film cooling hole is presented in Figure 1 and the detailed design variables are given in in Table 1.

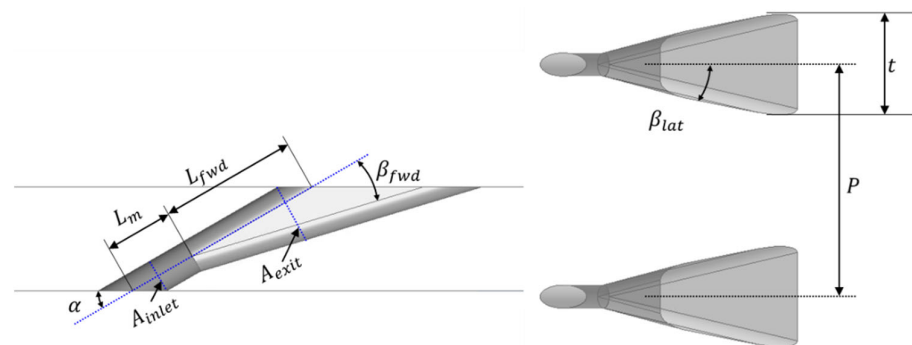


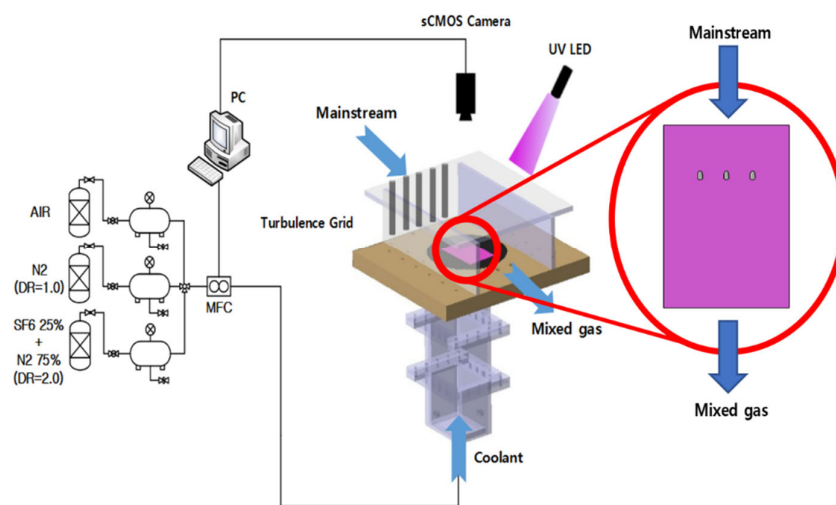
Figure 1. Geometry shape of the reference fan-shaped cooling hole [13].

Table 1. Reference fan-shape cooling hole dimensions [12].

Variable	Value
$L_{fwd}/D$	2.0
$L_m/D$	4.0
$A_{exit}/A_{inlet}$	13.24
$\beta_{fwd}$	13.3
$\beta_{lat}$	13.0
$P/D$	10
$t/D$	5.66

### 3. Test Apparatus

A detailed description of test apparatus has been presented by Park et al. [10]. Figure 2 shows a schematic of the test section for the film cooling performance measurement. The test section was designed so that the test plate mounted inside can be replaced. The test plates were additively manufactured by SLA (Stereolithography) method with a 0.05 mm layer thickness. The test plate has three identical holes, and the lateral distance between each hole was 10D. The test section was installed at the exit of a low-speed wind tunnel, and diameter of a circular cylindrical turbulence grid made is 9.5 mm and it is placed at 230 mm upstream from the film cooling hole trailing edge. The main flow properties were measured at the velocity measurement points indicated by red x marks in Figure 3. The flow properties along the vertical direction were measured using a hot-wire anemometer (Kanomax 1000 series). The mean velocity of the main flow was 20.0 m/s, measured boundary layer thickness was 3 mm, and mainstream turbulence intensity was 13%.



**Figure 2.** Schematic of film cooling test section [10].

Nitrogen ( $N_2$ ) and a mixture of SF6 (75% of  $N_2$  + 25% of SF6) were used as the foreign gas to simulate the density ratio of the coolant. The flow rate of the air and the foreign gas supplied to the film cooling hole through the plenum chamber was controlled by a mass flow controller (FMA-2600A, OMEGA). Two screens and a honeycomb were installed in the plenum chamber to supply the coolant to the holes uniformly. The PSP (Uni-FIB 400, ISSI) was coated uniformly throughout the test plate, and an LED array and a sCMOS camera (PCO edge 3.1, PCO) were installed on the top of the test section to measure the emitting intensity of the PSP. The uncertainty of the blowing ratio was estimated to be  $\pm 6.7\%$  when blowing ratio (BR) is 2.0 and density ratio (DR) is 2.0.

The uncertainty in measured film cooling effectiveness was calculated as  $\pm 7\%$  at the film cooling effectiveness of 0.3 and  $\pm 2\%$  at the film cooling effectiveness of 0.7. From the available measured data, measured data at BR = 1.0, 2.0 when DR = 2.0 were compared with LES results.

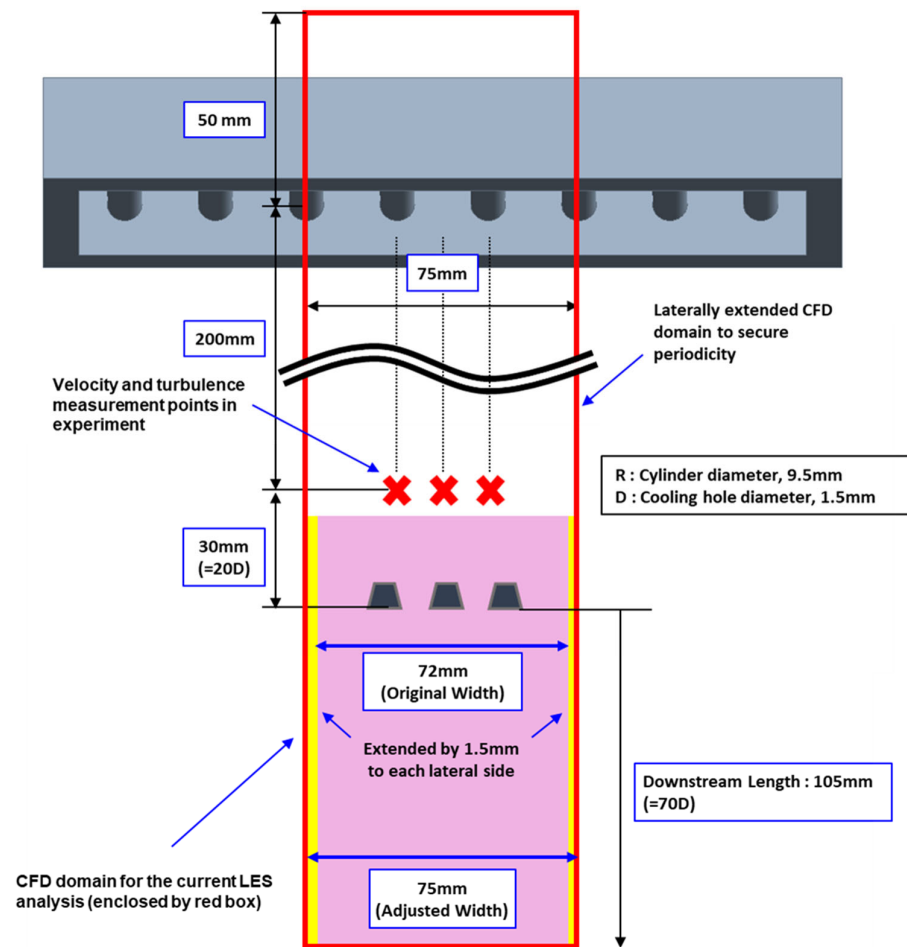


Figure 3. Top view of the CFD domain for the test section.

#### 4. Large Eddy Simulation

In this study, a commercial CFD code, Ansys CFX, has been used. Figure 3 depicts the computational domain (enclosed with red rectangular) of the test section. Cylinders with 9.5 mm diameter are located upstream of the film cooling hole to produce turbulence in the main flow as in the experiment. In the experiments, the width of the test plate, where the film cooling holes are located, was 72 mm and it has been extended by 1.5 mm (equivalent to 1D) toward each lateral side to satisfy the periodicity of the whole computational domain. Additionally, from the cooling hole downstream, the computational domain has been extended downstream by 105 mm (equivalent to 30D) to secure sufficient length for predicting cooling flow behaviors. In this study, LES analysis was performed in two steps as follows. At first, to validate feasibility of LES to resolve flow field downstream of the circular cylinder, two dimensional LES analysis including a row of circular cylinders has been carried out. Then, three dimensional LES analysis to predict the upstream turbulent boundary layer effect on the film cooling flow has been carried out.

##### 4.1. Two Dimensional LES Analysis

Before launching full three dimensional LES analysis, two dimensional LES analysis to resolve flow field around and downstream of the circular cylinder has been carried out. Figure 4 compares steady state RANS result with k-epsilon turbulence model and time-averaged LES result with WALE (Wall-Adapting Local Eddy-viscosity) sub-grid scale (SGS) model. The WALE SGS model is one of the major SGS models. It is an algebraic eddy viscosity model (0-equation model) as with the Smagorinsky SGS model, but it has some excellent features that the Smagorinsky model does not have. The WALE SGS model take the rotation rate into the calculation and it can handle the transition in the

calculation [15]. The RANS result does not show any repeating pattern of swirling vortices. Instead, there appears a long wake region downstream of the cylinder object. For this reason, the wake has been extended beyond the velocity measurement point (dotted line) and showed unrealistic velocity distributions at the behind the cylinder. Therefore, using the RANS method in the current study may derive physically invalid cooling flow behavior downstream of the cylinder row. On the other hand, repeating Karman vortex street stimulate mixing between low-speed region behind the cylinder and main flow region. For this reason, the wake region is shorter than RANS results. Moreover, at the velocity measurement point, more uniform velocity distributions were obtained.

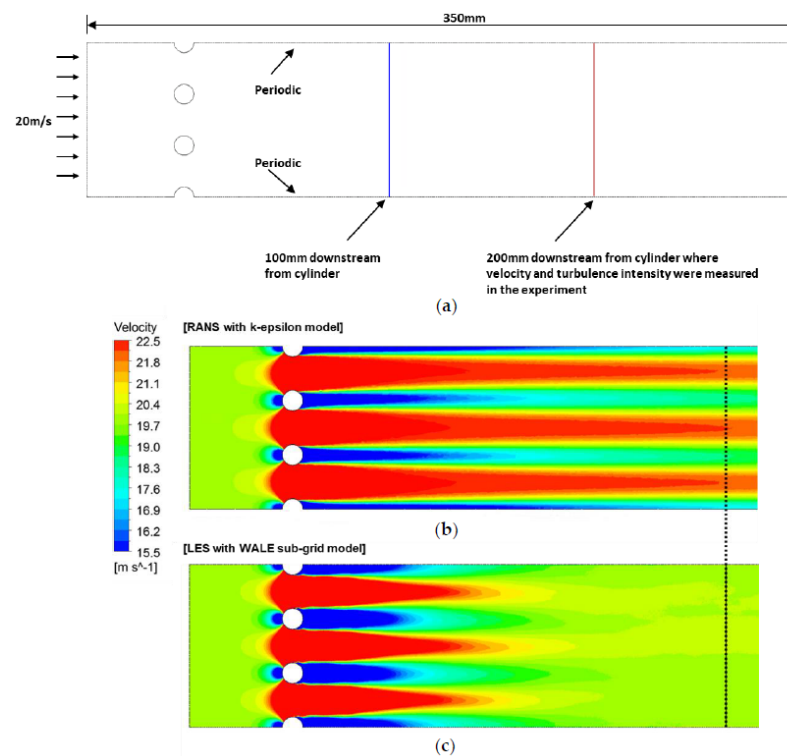


**Figure 4.** (a) Two dimensional CFD domain for validating circular cylinder downstream flow field; Comparison of velocity distributions between (b) steady state RANS with k–epsilon model and (c) LES with WALE sub–grid model.

Such a phenomenon frequently appears in CFD analysis for practical axial turbines, which generally have a relatively blunt trailing edge. In most cases, the wake initiated from the turbine trailing edge does not have a dominant effect on the whole flow field and turbine performance, even though it is recognized that the wake in the RANS analysis is not unrealistically extended toward downstream [16]. For assessing the performance turbine blades, this flow field behind the blade trailing edge can be neglected. However, as in this study, when the flow region of interest is included in wake, the RANS method cannot be used.

On the other hand, unsteady RANS could also predict the von Karman vortex shedding and behind the circular cylinder, however, their dissipation rate is higher than that of LES. Moreover, it is known that LES is more capable of predicting film cooling flow behaviors [2,3,7]. LES generally captures velocity field behind the cylinder successfully. For this reason, in this study, LES analysis has been used for predicting upstream circular cylinder effect on the film cooling flow on the flat plate, which is discharged far downstream of the circular cylinder row.

## 4.2. Numerical Simulation Descriptions for Three Dimensional LES Analysis

### 4.2.1. Mesh Generation

As shown in Figure 5, a three-dimensional CFD domain has been constructed including upstream downstream three fan shaped film cooling holes as well as upstream circular cylinders. As the grid independency test for LES is practically unreasonable, instead, the following criteria have been satisfied for LES mesh to resolve problem dependent eddies in current LES analysis.

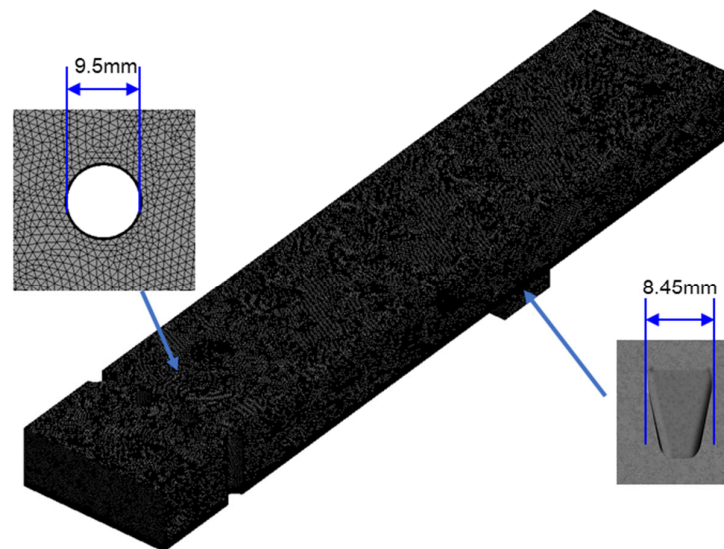


**Figure 5.** Computational meshes for the three-dimensional CFD domain including a row of circular cylinders and fan-shaped film cooling holes.

- The  $y^+$  value on the plate surface should be single digit to simulate proper boundary layer for the current simulation.
- $\Delta x^+$  and  $\Delta z^+$  values, evaluated based on the wall shear stress on the flat plate, are around 30.
- Non-dimensional turbulent boundary layer should be properly captured with given mesh distributions in front of the cooling hole. In this study, 13% main flow turbulent intensity should be captured in LES analysis.
- To capture problem dependent eddies, 15~20 elements are given in the boundary layer.

The definition of  $\Delta x^+$  is given by Equation (1):

$$\Delta x^+ = \frac{u^* dx}{\nu} \quad (1)$$

where  $u^*$  is shear velocity based on the wall shear stress,  $dx$  is element length in the  $x$ -direction, and  $\nu$  is kinematic viscosity, respectively.  $\Delta z^+$  can be evaluated in the same manner. The face size around the cooling hole has been adjusted to be  $0.1D$  and it satisfied above mentioned  $\Delta x^+$  and  $\Delta z^+$  criteria. The number of elements is 62,674,341 when satisfying above-mentioned mesh generation criteria. Figure 6a shows time averaged characteristic turbulence intensity along the vertical direction, defined in Equation (2).

$$I = \frac{\sum_1^N \sqrt{\frac{u'_i u'_i}{N}}}{U_\infty} \quad (2)$$

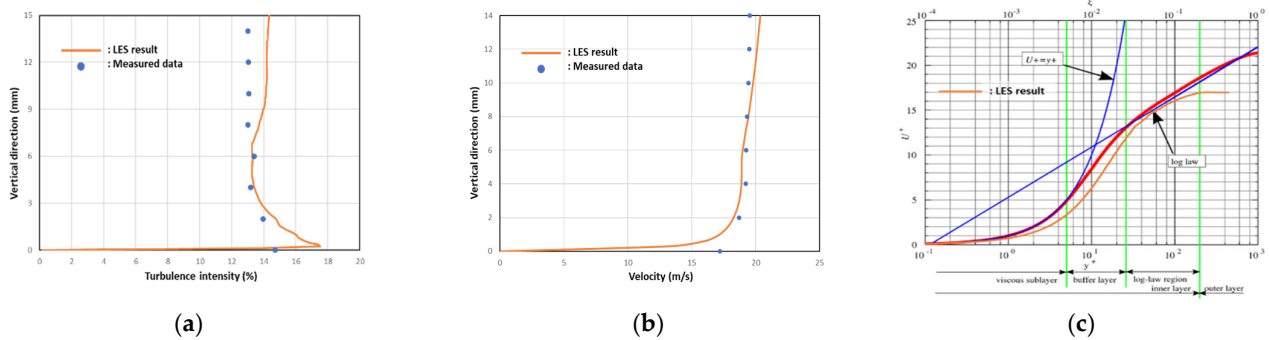


**Figure 6.** (a) Comparison of turbulence intensity, (b) velocity along the vertical direction, and (c) non-dimensional velocity distribution at the velocity measurement point.

The main flow turbulence intensity predicted at  $x/D = -20$  from the film cooling hole trailing edge is well agreed with measured turbulence intensity as shown in Figure 6a [13]. The characteristic turbulence intensity of the main flow was predicted around 13% to 15%. Additionally, higher turbulence intensity near the boundary layer is well predicted in the LES result as measured in the experiment. This means that the dissipation of Karman vortex street, originated from upstream cylinder, reasonably reflected to turbulence components in the current LES analysis. Figure 6b compares the velocity distributions between LES result and measured data along the vertical direction at  $x/D = -20$  from the film cooling hole trailing edge. From these two figures, the coolant upstream flow condition agrees well with the measured data. From Figure 6b, velocity distribution along the vertical direction up to 3D (4.5 mm) was extracted and normalized. Figure 6c shows normalized velocity distributions along the vertical direction. The velocity was normalized based on the time-averaged streamwise velocity and wall shear stress to evaluate  $y^+$  and  $u^+$ . Kang et al. [9] showed that without any turbulence generation method at upstream of the cooling hole, the normalized boundary layer follows viscous sublayer and its extension in LES analysis, where  $y^+$  is  $u^+$ . In this study, due to the upstream Karman vortex street effect, the approaching boundary layer is close to the Spalding's law. It means that the approaching boundary layer is fully developed and proper upstream turbulent boundary layer is reasonably simulated in the current LES analysis.

#### 4.2.2. Boundary Conditions

Boundary conditions for the current LES analysis are described in Figure 7. At the main flow inlet, both turbulent velocity profile and bulk velocity were tried as inlet boundary conditions. However, static turbulent velocity profile was not effective for generating boundary layer vortex in LES. For this reason, turbulence components bulk velocity and temperature values were specified for the main flow inlet boundary conditions, for simplicity. At the main flow outlet, atmospheric static pressure was given. The mass flow and the constant temperature were specified at the coolant inlet chamber. The blowing ratio were adjusted by varying mass flow rate. In this study, LES analyses at two different blowing ratios have been carried out.

$$DR = \rho_c / \rho_\infty = 2.0 \quad (3)$$

$$BR = \rho_c U_c / \rho_\infty U_\infty = 1.0, 2.0 \quad (4)$$

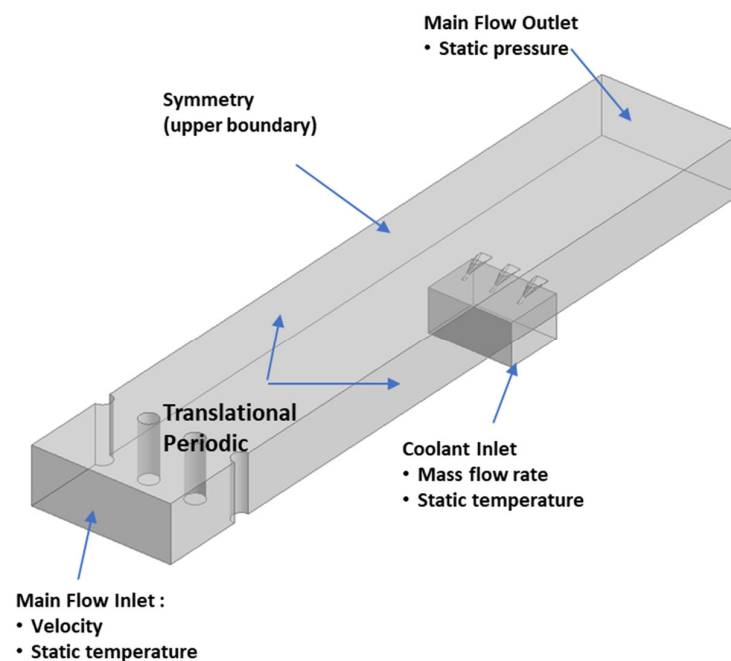


**Figure 7.** Boundary conditions for the three-dimensional CFD domain including a row of circular cylinders and fan-shaped film cooling holes.

Subscript  $c$  and  $\infty$  in Equations (3) and (4) mean cooling flow and main flow, respectively. WALE sub-grid model was chosen to simulate turbulence less than element size. A second-order central differential discretization scheme was chosen for the advection term of the governing equation to predict physically valid diffusion of generated eddies in the LES analysis. Bound ed CDS option has been enabled to improve the stability of the analysis. As the LES analysis is inherently unsteady simulation, a physical time-step should be given. To secure the numerical stability in the LES analysis, the physical time-step was defined so that the overall CFL number was not more than 0.75. Under this configuration, five internal-loops were set in each physical time-step. As an initial condition for each LES analysis at different blowing ratio, steady-state RANS simulation results with SST turbulence model were given. The time average was started after the RANS simulation result completely disappeared downstream. The maximum number of timesteps was set for the main flow to secure six through time of the main flow from the main flow inlet to the main flow outlet.

## 5. Numerical Simulation Results

### 5.1. Turbulent Boundary Layer Effect on the Film Cooling Effectiveness

Figure 8 shows the instantaneous vorticity distribution when the blowing ratio is 2.0. In the main flow region, a clear Karman vortex street appears behind the circular cylinder. The Karman vortex street in the main flow region dissipates quickly compared to the boundary layer. In the boundary layer, the bulk Karman vortex street splits into the small vortex structure and flows downstream and becomes turbulent components in the boundary layer.

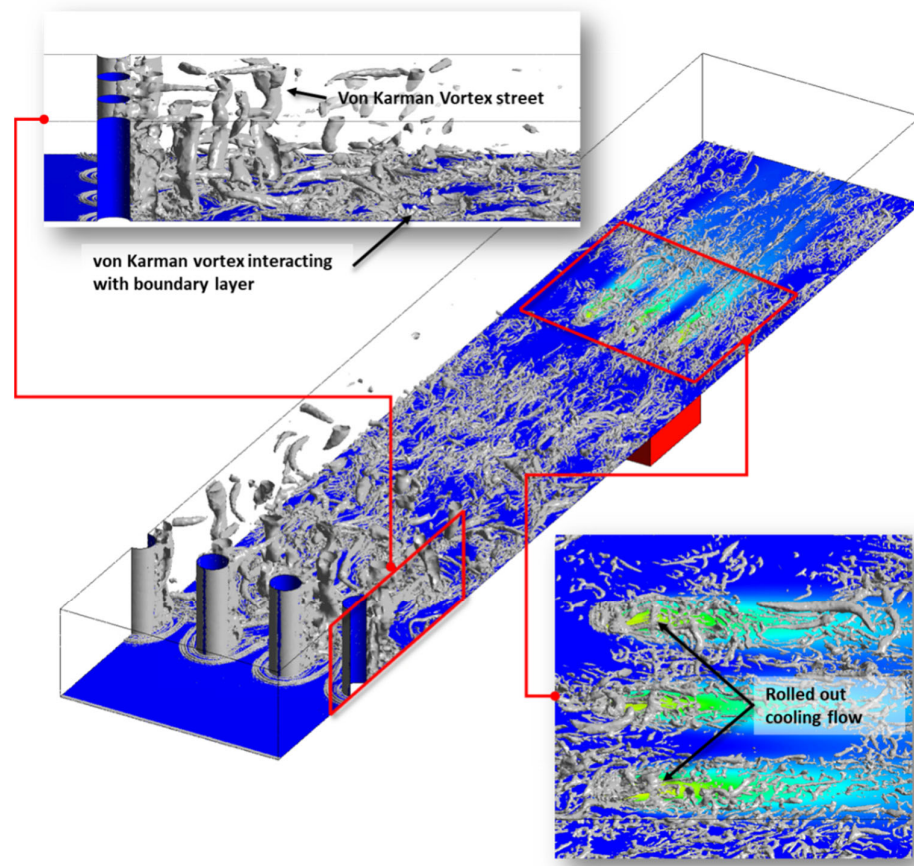


**Figure 8.** Instantaneous vortex structures when the blowing ratio is 2.0.

The strength of the vortex structure near the boundary layer in front of the cooling hole is similar order that of the vortex structure from the injected cooling flow. Interaction between these two-vortex structure results in the effective area of the cooling flow distributions shown in Figure 8.

Contours of adiabatic film cooling effectiveness, defined in Equation (5), around the film cooling hole were compared with measured data.

$$\eta = \frac{T_{\infty} - \overline{T}_w}{T_{\infty} - T_c} \quad (5)$$

where  $T_{\infty}$  is main flow temperature,  $\overline{T}_w$  is time averaged wall temperature, and  $T_c$  is cooling flow temperature, respectively. Figure 9 shows film cooling effectiveness distributions with and without upstream turbulence in the boundary layer when the blowing ratio is 2.0. One interesting thing is that when there is no upstream turbulence effect, then the effective area of the cooling flow was far extended toward downstream. When the boundary layer is turbulent, then the coverage of the cooling flow becomes shorter. Moreover, near the cooling hole trailing edge, a high adiabatic cooling effectiveness region appears at the lateral side of the cooling hole in Figure 9a; however, this region disappears when the boundary layer is turbulent. Kang et al. [9] reasoned that that when the boundary layer is laminar, then the laminar boundary layer developed into the horseshoe vortex at the cooling hole leading edge and the horseshoe vortex flows along the lateral edge of the cooling without dissipating. On the other hand, due to the characteristic of the fan-shaped film cooling hole, the cooling flow is also injected into the lateral direction. Then, the horseshoe vortex kept the laterally injected cooling flow from lift-off or dissipation. For this reason, there appears high film cooling effectiveness region at the lateral side of the cooling hole when there is no turbulence information in the boundary layer. However, when the

boundary layer is turbulent, the horseshoe vortex, initiated from the cooling hole, is no longer strong enough to suppress the lift-off of the cooling flow injection toward the lateral direction. Additionally, turbulence promotes lift-off of the cooling flow and its mixing with the main flow. For this reason, the coverage of the cooling flow is reduced. Kang et al. also showed that the boundary layer turbulence has a significant effect on the effective range of the film cooling flow. From this point of view, the turbulence information due the upstream circular cylinder in the current numerical simulation and its interaction with the cooling flow are reasonably predicted in the current LES analysis.

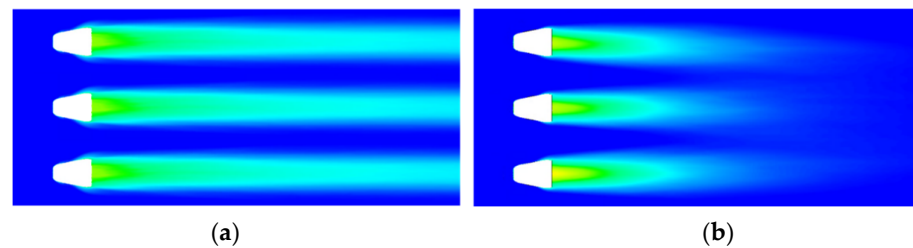


**Figure 9.** Comparison of film cooling effectiveness distributions (a) without and (b) with upstream turbulence in the boundary layer when the blowing ratio is 2.0.

Figure 10a shows the laterally averaged film cooling effectiveness distribution along the stream-wise direction. Except for the region where  $x/D$  is around 5, the laterally averaged film cooling effectiveness without upstream turbulence is about 0.02 higher in other stream-wise locations. Figure 10b shows film cooling effectiveness distributions along the centerline. Along the centerline, the difference between film cooling effectiveness without upstream turbulence effect and without upstream turbulence effect is more pronounced at the downstream. This means as the coolant flows downstream, the cooling flow interacts more actively with the turbulent boundary layer. As a result, there appears the rapid cooling flow dissipation to the main flow, and it limits the effective range of the cooling flow over the flat plate.

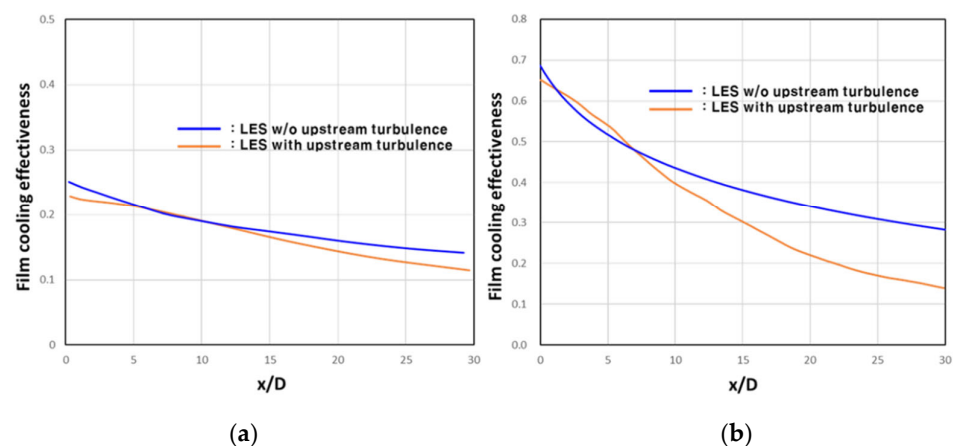


**Figure 10.** (a) Laterally averaged film cooling effectiveness distribution and (b) film cooling effectiveness along the centerline at the blowing ratio of 2.0 according to the upstream turbulence.

### 5.2. Film Cooling Effectiveness Distributions on the Flat Plate

Figure 11 compares film cooling effectiveness between measured data and LES results according to the blowing ratio. LES results predicted reasonable coverage of the film cooling effectiveness over the flat plate when compared with measured data. When the blowing ratio is 1.0, both in measured data and LES result, the coverage of the cooling flow is limited just downstream the cooling hole trailing edge. As the blowing ratio increases, the increased amount of cooling flow covered wider range at downstream area. A direct influence of the film cooling flow on the flat plate and its dissipating toward

the main flow were well reflected on the film cooling effectiveness distribution on the flat plate both in the measured data and LES results. The qualitative distributions of the film cooling effectiveness in LES results according to the blowing ratio are well agreed with corresponding measured film cooling effectiveness. This means that the LES method is a competitive method to predict film cooling flow behaviors as well as its interaction with turbulent boundary layer over a flat plate when there is a turbulence source inside the computational domain.

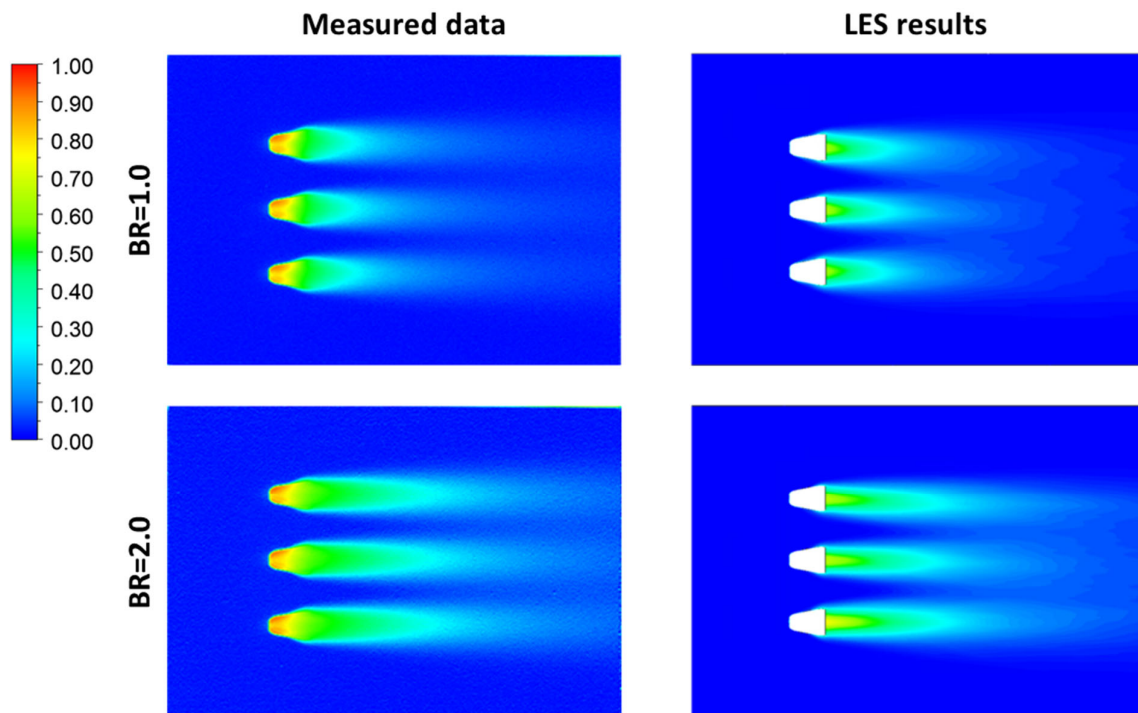


**Figure 11.** Comparison of film cooling effectiveness distribution between measured data and LES results according to the blowing ratio.

### 5.3. Film Cooling Effectiveness at Chosen Locations

To compare the quantified film cooling effectiveness distribution on the flat plate from the LES results with measured data, the following values were evaluated:

- Laterally averaged film cooling effectiveness distribution between  $0 < x/D < 30$
- Centerline film cooling effectiveness distribution between  $0 < x/D < 30$
- Lateral distribution of film cooling effectiveness at  $x/D = 2, 5, 10$  and  $20$

Figure 12 shows laterally averaged film cooling effectiveness distributions along the streamwise direction when the blow ratio is 1.0 and 2.0. When the blowing ratio is 1.0, LES result and measured data well agree at the cooling hole trailing edge. As  $x/D$  increases, there appears discrepancy between LES result and measured data up to 0.03. At the far downstream where  $x/D$  is over than 20, then this discrepancy between LES result and measured data decreases again. When the blowing ratio is 2.0, lower film cooling effectiveness compared to measured data by 0.07 was predicted by LES results and as  $x/D$  increases this discrepancy also decreases and maintain the offset these two results by 0.02. Figure 13 shows the film cooling effectiveness along the centerline. At both blowing ratio, the film cooling effectiveness near the cooling hole trailing edge is higher than that of the measured data. As the  $x/D$  increases, such as the laterally averaged film cooling effectiveness distributions presented above, discrepancies LES results and measured data reduce.

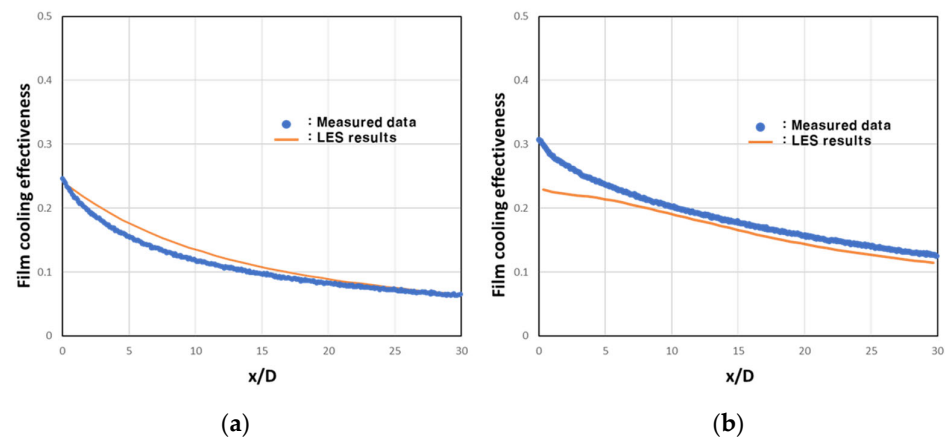


**Figure 12.** Laterally averaged film cooling effectiveness distributions at (a) BR = 1.0 and (b) BR = 2.0.

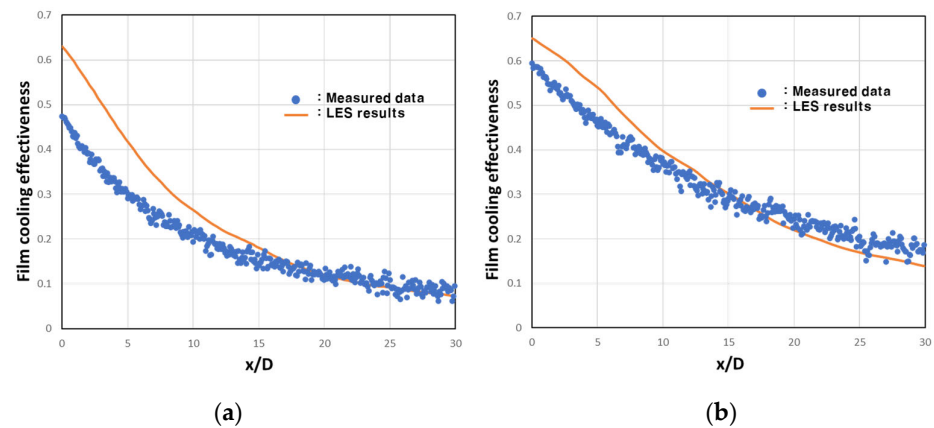


**Figure 13.** Film cooling effectiveness distributions along the centerline at (a) BR = 1.0 and (b) BR = 2.0.

This means that the centerline film cooling effectiveness is over-predicted by LES results and the laterally averaged film cooling effectiveness is similar or less predicted by LES analyses.

Figure 14 shows lateral distributions of the film cooling effectiveness at those locations of  $x/D$  when the blowing ratio is 1.0. At  $x/D = 2.0$ , near the centerline, the numerically predicted film cooling effectiveness is higher than measured data by 0.15. High film cooling effectiveness region is concentrated near the centerline and the cooling flow is more widely distributed and uniform in the measured data. This over-prediction in the LES result is decreasing as the flow goes downstream. At the  $x/D = 20$  in Figure 14d, in both measured data and LES result, the most cooling flow was dissipated along the lateral and vertical direction. Measured data and the LES results agree very well along the lateral location as well as at the centerline. A similar trend appeared in Figure 15 when the blowing ratio is 2.0.

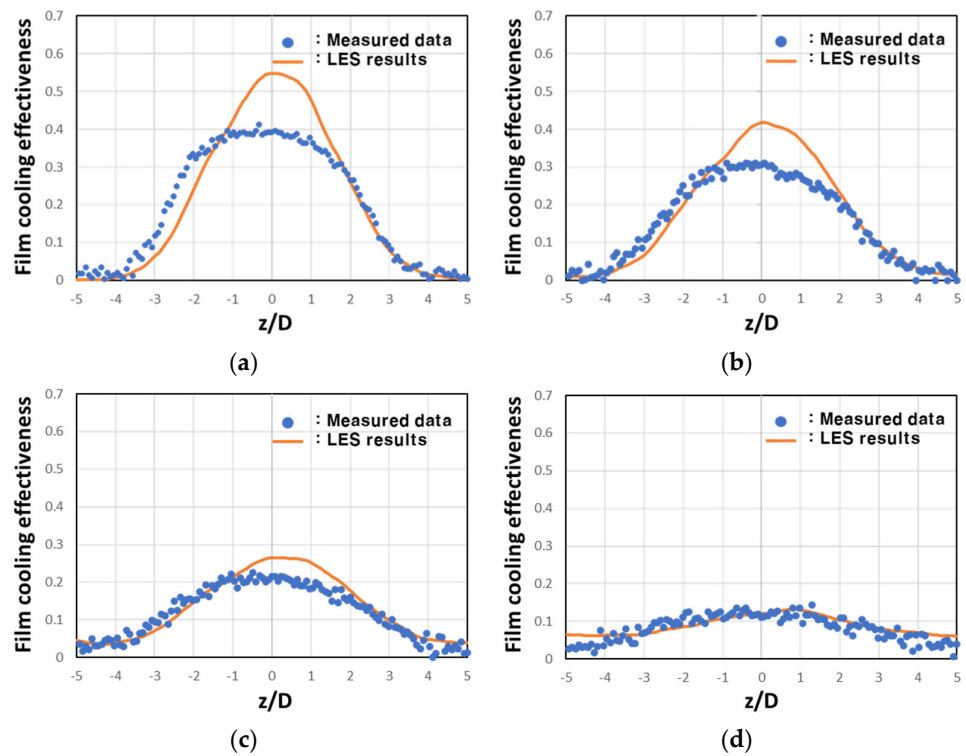


Figure 14. Lateral film cooling effectiveness distributions at (a)  $x/D = 2$ , (b)  $x/D = 5$ , (c)  $x/D = 10$ , and (d)  $x/D = 20$  when the blowing ratio is 1.0.

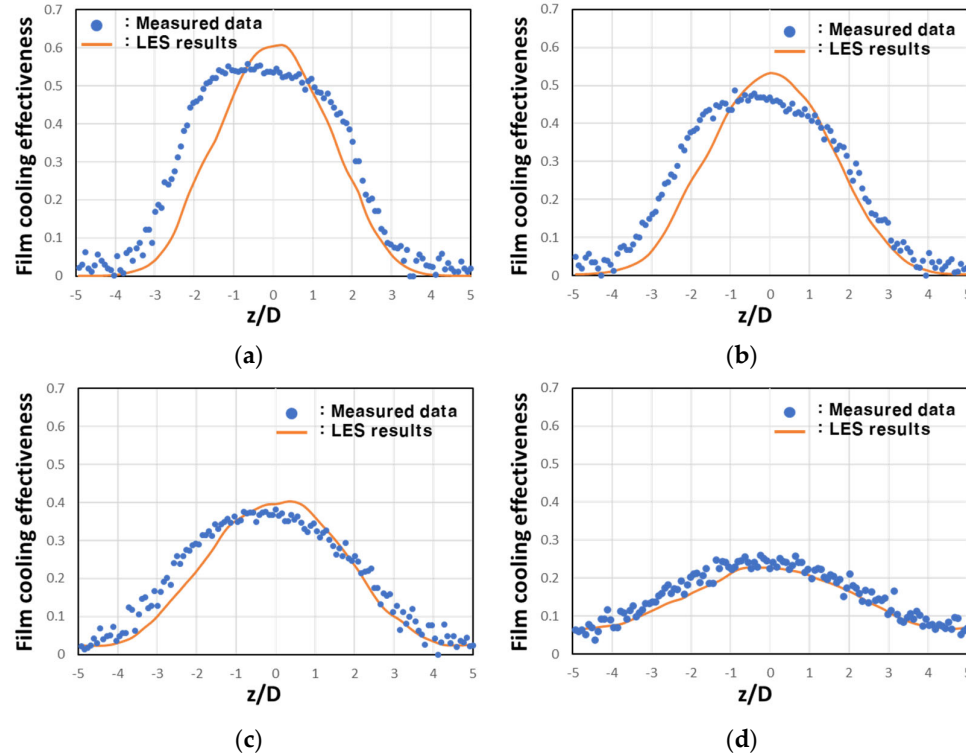
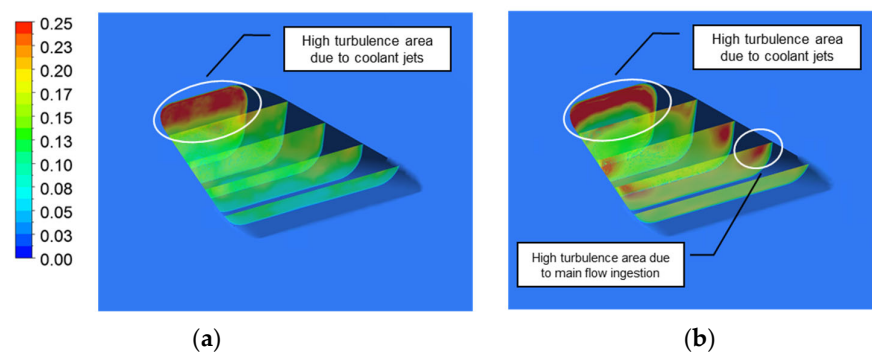


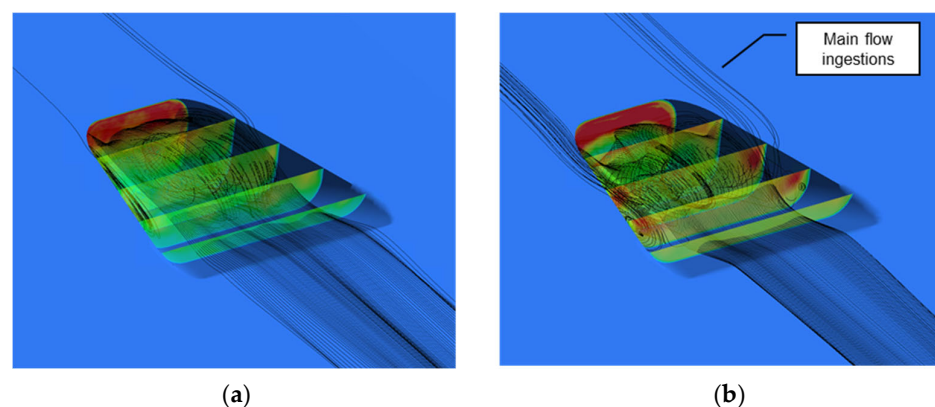
Figure 15. Lateral film cooling effectiveness distributions at (a)  $x/D = 2$ , (b)  $x/D = 5$ , (c)  $x/D = 10$ , and (d)  $x/D = 20$  when the blowing ratio is 2.0.

Figure 16 compares the characteristic turbulence intensity inside the cooling hole section by section between the leading edge and the trailing edge of the cooling hole. Without the upstream turbulent boundary layer, the boundary layer flow ingestion to the

film cooling hole is not strong due to the horseshoe vortex in front of the cooling hole leading edge. Only the turbulence intensity near the cooling hole leading is high because of the coolant jets. On the other hand, when the turbulent boundary layer is approaching, the strong horse vortex no longer sustains at the cooling hole leading edge. Moreover, it no longer keeps the boundary layer flow from ingesting into the cooling hole. At the lateral location in the cooling hole, the characteristic turbulence was predicted to an also very high value as shown in Figure 16b. Figure 17 compares streamline distributions along with turbulence intensity without and with upstream turbulent boundary layer. Without the upstream turbulent boundary layer, the boundary layer flow is hardly ingested into the cooling hole. However, when the upstream boundary layer is turbulent, the boundary layer flow ingested into the cooling hole from the lateral sides and circulates inside the cooling hole. The ingested flow accumulates near the center of the cooling hole and discharges again into the main flow while mixing with the cooling flow. By this procedure, the cooling flow was also induced along the centerline. This results in the high centerline cooling effectiveness distributions in the current LES analysis compared to the measured data, as shown in Figures 14a and 15a.



**Figure 16.** Characteristic turbulence intensity inside the cooling hole (a) without and (b) with upstream turbulent boundary layer when the blowing ratio is 2.0.



**Figure 17.** Streamline distributions inside the cooling hole (a) without and (b) with upstream turbulent boundary layer when the blowing ratio is 2.0.

Table 2 summarizes the area-averaged film cooling effectiveness where  $x/D$  is from 0 to 30. Compared to the measured film cooling effectiveness, area averaged film cooling effectiveness at  $BR = 1.0$  well agrees with the measured data, even though there are local discrepancies. The lower film cooling effectiveness at  $BR = 2.0$  has been predicted by LES analysis.

**Table 2.** Comparison of area averaged film cooling effectiveness.

Blowing Ratio	Measured Data	LES Result
1.0	0.118	0.118
2.0	0.184	0.165

One of the reasons for lower film cooling effectiveness in the LES results came from higher turbulence intensities in the boundary layer compared to the measured data as shown in Figure 6a. Higher turbulence intensity in the boundary layer could cause early dissipation especially at higher BR in the LES results and corresponding reduced coverage compared to the measured data. Additionally, over-prediction in the centerline film cooling effectiveness compared to the measured data could be another reason. As the cooling flow was concentrated to the centerline, the cooling flow did not spread to the lateral direction close to the cooling hole. However, discrepancy of area averaged film cooling effectiveness is less than 0.02, which is very reasonable prediction compared to the RANS results.

## 6. Conclusions

From this study, the following conclusions could be drawn:

- To numerically simulate von Karman vortex street and resultant high turbulence components in the main flow, the LES method is essential. As in this study, when the size of turbulator (circular cylinder in this study) is larger than the problem dependent geometry (diameter of fan shaped cooling hole) and eddy size (vortex structures originated from the cooling hole), RANS was unable to resolve the physically reasonable circular cylinder downstream flow field. The LES method reasonably predicted cylinder downstream velocity and turbulence components.
- The LES predicted reasonable interaction between the cooling flow and turbulent boundary layer, and corresponding film cooling effectiveness distributions. The turbulent boundary layer promotes early dissipation of the cooling flow injected from the cooling hole.
- Due to approaching turbulent boundary layer, the main flow is ingested into the cooling hole and this results in deteriorated film cooling effectiveness distributions on the surface of the cooling hole. Moreover, the ingested main flow is recirculating and accumulates near the centerline, then induces the cooling flow along the centerline. This results in the high film cooling effectiveness distributions along the centerline in the LES results.
- Overall, the difference of area-averaged film cooling effectiveness between LES results and measured data is less than 0.02 for the current study, and it can be stated that LES results and measured data show reasonable agreement.

**Author Contributions:** Methodology, investigation, visualization, writing—original draft preparation, Y.J.S.; software, validation, investigation, writing—original draft preparation, Y.S.K. Writing—Review, D.-H.R.; conceptualization, supervising and writing—review, J.S.K. All authors have read and agreed to the published version of the manuscript.

**Funding:** This work was funded by the Ministry of Industry, Trade & Energy (Republic of Korea) through the Aerospace Component Technology Development Program (Grant No. 10083654).

**Institutional Review Board Statement:** Not applicable.

**Informed Consent Statement:** Not applicable.

**Data Availability Statement:** Not available.

**Acknowledgments:** This work was supported by the National Supercomputing Center with supercomputing resources including technical support (KSC-2020-CRE-0036).

**Conflicts of Interest:** The authors declare no conflict of interest.

## References

1. Li, S.; Zhan, J.; Gong, Y.; Hu, W. Numerical Investigation of Film Cooling Using RANS and LES. *Procedia Eng.* **2015**, *126*, 701–705. [[CrossRef](#)]
2. Dickhoff, J.; Schneider, M.; Horiuchi, K.K.T.; Fukuda, M.; Bohn, D. Comparison between RANS and Large Eddy Simulations for Nekomimi- and 777-Shaped Film Cooling Holes. In Proceedings of the International Gas Turbine Congress 2019, Tokyo, Japan, 17–22 November 2019. IGTC-2019-148.
3. Kang, Y.S.; Jun, S.; Rhee, D. Large Eddy Simulations on Film Cooling Flow from a Fan-Shaped Cooling Hole on a Flat Plate, The KSFM. *J. Fluid Mach.* **2018**, *21*, 5–13.
4. Tracy, K.; Lynch, S.P. Large Eddy Simulation of the 7-7-7 Shaped Film Cooling Hole at Axial and Compound Angle Orientations. In Proceedings of the ASME Turbo Exposition, Online, 21–25 September 2020. ASME Paper No. GT2020-14439.
5. Jee, S.; Joo, J.; Lin, R. Toward Cost-Effective Boundary Layer Transition Computations with Large-Eddy Simulation. *J. Fluids Eng.* **2018**, *140*, 111201. [[CrossRef](#)]
6. Kang, S.Y.; Jun, S.; Rhee, D. Large Eddy Simulations on Fan Shaped Film Cooling Hole with Various Inlet Turbulence Generation Methods. In Proceedings of the ASME Turbo Exposition, Online, 21–25 September 2020. ASME Paper No. GT2020-15830.
7. Nikolaos, S. Large Eddy Simulation of the Film Cooling Flow System of Turbine Blades: Public Shaped Holes. Master's Thesis, Institut Supérieur de l'Aéronautique et de l'Espace, Toulouse, France, 2016.
8. Menter, F.R.; Garbaruk, A.; Smirnov, P.; Cokljat, D.; Mathey, F. Scale-Adaptive Simulation with Artificial Forcing. In *Progress in Hybrid RANS-LES Modelling. Notes on Numerical Fluid Mechanics and Multidisciplinary Design*; Peng, S.H., Doerffer, P., Haase, W., Eds.; Springer: Berlin/Heidelberg, Germany, 2010; pp. 235–246.
9. Kang, Y.S.; Jun, S.; Rhee, D. Large Eddy Simulations on Fan Shaped Film Cooling Hole with Upstream Boundary Layer Turbulence Effect Generated by Trip Strip. *J. Therm. Sci. Eng. Appl.* **2022**, *14*, 031006. [[CrossRef](#)]
10. Park, S.H.; Kang, Y.J.; Seo, H.J.; Kwak, J.S.; Kang, Y.S. Experimental optimization of a fan-shaped film cooling hole with 30 degrees-injection angle and 6-hole length-to-diameter ratio. *Int. J. Heat Mass Transf.* **2019**, *144*, 118652. [[CrossRef](#)]
11. Nishino, T.; Roberts, G.T.; Zhang, X. Unsteady RANS and detached-eddy simulations of flow around a circular cylinder in ground effect. *J. Fluids Struct.* **2008**, *24*, 18–33. [[CrossRef](#)]
12. Song, Y.J.; Park, S.; Kang, Y.; Kwak, J. Effects of trench configuration on the film cooling effectiveness of a fan-shaped hole. *Int. J. Heat Mass Transf.* **2021**, *178*, 121655. [[CrossRef](#)]
13. Seo, H.J.; Park, S.H.; Kwak, J.S.; Kang, Y.S. Experimental and Numerical Study on The Effect on Fan-Shaped Hole Configuration on Film Cooling Effectiveness. In Proceedings of the ASME Turbo Exposition, Phoenix, AZ, USA, 17–21 June 2019. ASME Paper No. GT2019-90817.
14. Schroeder, R.P.; Thole, K.A. Adiabatic Effectiveness Measurements for a Baseline Shaped Film Cooling Hole. In Proceedings of the ASME Turbo Exposition, Düsseldorf, Germany, 16–20 June 2014. ASME Paper No. GT2014-25992.
15. Nicoud, F.; Ducros, F. Subgrid-Scale Stress Modelling Based on the Square of the Velocity Gradient Tensor. *Flow Turbul. Combust.* **1999**, *62*, 183–200. [[CrossRef](#)]
16. Dufour, G.; Gourdain, N.; Duchaine, F.; Vermorel, O.; Gicquel, L.Y.M.; Boussuge, J.-F.; Poinot, T. *Numerical Investigations in Turbomachinery: A State of the Art Large Eddy Simulation Applications*; VKI Lecture Series; CERFACS: Toulouse, France, 2009.